Weak Antilocalization in a Strongly Disordered Two-Dimensional Semimetal in an HgTe Quantum Well

© E.B. Olshanetsky[1], Z.D. Kvon[1,2], N.N. Mikhailov[1]

[1] Institute of Semiconductor Physics Siberian Branch
Russian Academy of Sciences,
630090 Novosibirsk, Russia
[2] Novosibirsk State University,
630090 Novosibirsk, Russia

E-mail: eolsh@isp.nsc.ru

Received July 30, 2023
Revised August 4, 2023
Accepted August 4, 2023

Weak localization in a highly disordered quantum well $Cd_xHg_{1-x}Te/HgTe/Cd_xHg_{1-x}Te$ with a thickness of $d = 20$ nm is experimentally investigated. An analysis is made of the anomalous positive magnetoresistance (APM) caused by the suppression of the interference correction to the conductivity by a magnetic field on both sides of the charge neutrality point: for a two-dimensional semimetal and for a two-dimensional electronic metal. For the same values of resistivity, the APM peak in a 2D semimetal has a much wider width than in a 2D electron gas. A quantitative comparison of the obtained results with the theory allows, in particular, to conclude that the intensity of carrier transitions between subsystems in the 2D semimetal binary system is maximum near the charge neutrality point, where the concentrations of electrons and holes are close, and decreases as the difference in concentrations increases.

Keywords: semimetal, quantum well, HgTe, weak antilocalization.

1. Introduction

Gapless semiconductors such as HgTe are unique objects. The use of quantum wells (QWs) of various thicknesses made on their basis makes it possible to produce a wide variety of two-dimensional electron and hole systems. It has now been established that when the QW thickness of HgTe is below the critical value of $d < d_c \approx 6.5$ nm, a two-dimensional electron system with a normal band spectrum and a normal band gap is realized in it. A HgTe quantum well of critical thickness is a system of two-dimensional Dirac fermions with a gapless dispersion law, which is linear in respect to the wave vector k [1]. A QW with a thickness slightly greater than the critical value, $d > d_c$, has an inverted band spectrum and is a so-called two-dimensional topological insulator, that is a system with a band gap for bulk states and gapless edge states circulating along the edge of the sample [2–5]. With a further increase in thickness ($d > 14$ nm), the QW retains an inverted band spectrum (Figure 1, *c*) where the conduction band and the valence band are formed, respectively, by two-dimensional subbands *hh*1 and *hh*2, arising as a result of size quantization of the heavy hole band of bulk mercury telluride, and the electron-like two-dimensional subband *s*1 (not shown in the figure) is located at a lower energy level [6]. As can be seen from the figure, an important feature of the wide ($d > 14$ nm) wells of HgTe is the gapless energy spectrum, characterized by the overlap of the bottom of the conduction band *hh*1 located in the center of the Brillouin zone with the side maxima of the valence band *hh*2.

Among the various studies of electron transport in HgTe QWs, an important place is occupied by the observation of effects caused by the interference of the wave function of charge carriers in the well. These include, in particular, interference quantum corrections to conductivity and associated localization and antilocalization types of magnetoconductivity observed in weak magnetic fields. Experimental studies of interference effects in HgTe quantum wells of various thicknesses have been ongoing for more than ten years. Thus, similar effects were studied near the topological transition for electrons in the conduction band in QWs with both inverted ($d > d_c$) and normal ($d < d_c$) spectrum [7,8], for holes in a QW with a normal spectrum [9], for two-dimensional Dirac fermions in a QW of critical thickness [10], as well as in a three-dimensional topological insulator based on strained HgTe films with thicknesses of 80 and 200 nm [11,12]. The main feature of these effects, regardless of the well thickness, type of carriers and energy spectrum, is the observation of pronounced weak antilocalization, indicating rapid spin relaxation due to the strong spin-orbit interaction in these structures. An equally important feature of these structures is the ability to observe weak localization effects in the presence of several different types of charge carriers at once. Thus, in [9] quantum interference corrections to hole conductivity in the valence band were observed under conditions when, due to the strong spin-orbit splitting of this band, the transfer was performed by two types of holes. At the same time, a three-dimensional topological insulator based on thick strained HgTe films [11,12] is a system where two-dimensional Dirac fermions on the upper and lower surfaces of the sample

can be simultaneously present together with ordinary two-dimensional holes and electrons in bulk valence band and conduction band.

In this context, the study of weak antilocalization effects in wide ($d > 14$ nm) HgTe quantum wells (QWs) is of significant interest. In samples based on them, equipped with an electrostatic gate, it is possible to move the Fermi level from the conduction band, where the only type of charge carriers are electrons, to the region of overlap of the conduction band and valence band, where two types of carriers are simultaneously present in the QW: electrons and holes, i.e. a two-dimensional semimetal is realized (see diagrams in Figure 2) [13,14]. This study presents the results of investigation of features of the magnetotransport caused by the suppression by a weak magnetic field of interference quantum corrections to the conductivity in a bulk doped 20 nm HgTe quantum well. The wide range of gate voltages used made it possible to investigate the behavior of weak antilocalization both in the case of a two-dimensional electron gas in the conduction band and in a two-dimensional semimetal. As a result of comparing experiment with theory, the parameters characterizing systems of two-dimensional electrons and two-dimensional semimetal were determined.

2. Samples

To prepare experimental samples, a 20 nm QW of $Cd_xHg_{1-x}Te/HgTe/Cd_xHg_{1-x}Te$ with $x = 0.74$ and (013) orientation of the surface, which layer-by-layer structure is shown in Figure 1, *a*. The main feature of this well, in comparison with previously studied similar wells, is the presence of an additional disorder created by bulk doping of the QW with indium ($n_{In} \approx 10^{17}$ cm^{-3}) to enhance the relative magnitude of the quantum correction to the measured resistance due to a decrease in mobility. Based on this QW, Hall bridges with a width of $W = 50\,\mu$m and a distance between potentiometric contacts of 100 and 250 μm were fabricated using optical lithography and plasma-chemical etching (Figure 1, *b*). Ohmic contacts to the two-dimensional electron system in the QW were achieved by burning indium onto the contact pads. To fabricate a gate on the structure, a dielectric layer consisting of 100 nm SiO_2 and 200 nm Si_3N_4 was first grown on the structure. Then, the TiAu gate was deposited. The change in charge carrier density in the QW with variation of the gate voltage was $1.09 \cdot 10^{15}$ m^{-2}/V. Magnetotransport measurements in the described structures were carried out at a temperature of ≈ 200 mK, in weak magnetic fields of < 1 T, at a frequency of 13 Hz, in a standard four-point configuration.

3. Results and discussion

Figure 2 shows the sample resistivity as a function of the gate voltage in a zero magnetic field. Form of the

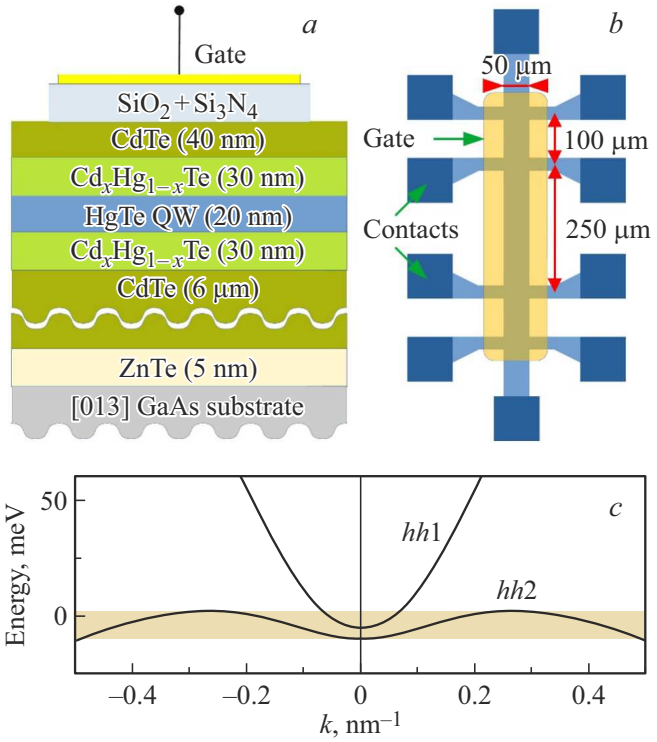

Figure 1. *a* — layer-by-layer structure of the quantum well; *b* — top view of the sample; *c* — schematic representation of the band spectrum of a 20 nm HgTe QW. The area of conduction band and valence band overlap is highlighted. (The colored version of the figure is available on-line).

dependence is typical for wide HgTe QWs. At high positive biases on the gate, the Fermi level is located in the conduction band, but above the side maxima of the valence band, and therefore outside the overlap region of these bands (see the diagram on the right in Figure 2). In this case, a two-dimensional electron metal with a relatively high concentration and mobility of carriers is realized in the sample. When the gate voltage changes from positive to negative value, the Fermi level drops and at some point crosses the top of the valence band, while remaining in the conduction band. In this case, the resistance increases and reaches a maximum at a gate voltage that corresponds to the approximate equality of electrons in the conduction band and holes in the valence band — at the so-called charge neutrality point (CNP): ($V_{CNP} \approx -1.25$ V). With a further increase in the negative bias up to its maximum values, the Fermi level drops lower in the valence band, but at the same time, due to the high density of states in the valence band, it does not leave the conduction band (see the diagram on the left in Figure 2). Thus, starting from the gate voltages corresponding to CNP and for all gate voltages to the left of it, the QW simultaneously contains both holes in the valence band and electrons in the conduction band, i.e. the state of a two-dimensional semimetal is realized.

Analysis of the magnetofield dependences $\rho_{xx}(B)$ and $\rho_{xy}(B)$ in classically weak magnetic fields using the Drude

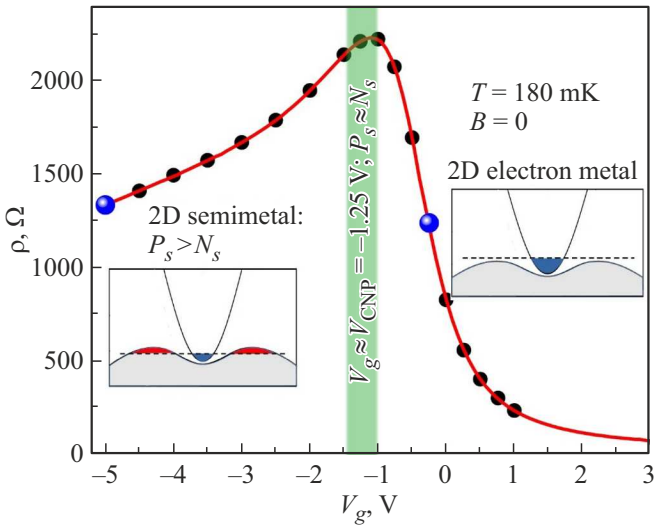

Figure 2. Sample resistance as a function of gate voltage at $B = 0$. The area of the charge neutrality point is highlighted in green. Black symbols indicate the magnetic field values for which the magnetic field dependences were measured. Blue symbols highlight points with close values of $\rho(B = 0)$, for which the behavior of AMR is compared in Figure 4. (The colored version of the figure is available on-line).

model for a system with two types of charge carriers makes it possible to plot dependences of the concentration and mobility of electrons and holes for gate voltages corresponding to position of the Fermi level in the band overlap region. Figure 3, *a* and *b* show the dependences obtained in this way, as well as similar dependences for the two-dimensional electron metal to the right of V_{CNP}. Using the obtained dependences, it is also possible to determine the dependence of the hole σ_h and electron σ_e contributions to the total conductivity of the system σ_{total} on the gate voltage (Figure 3, *c*). We will need these dependencies later.

Over the entire available gate voltage range, i. e. both for its values corresponding to the state of a two-dimensional electron gas, and for those at which the state of a two-dimensional semimetal is realized, the behavior of $\rho(B)$ demonstrates typical features that are usually associated with the suppression of interference corrections to conductivity by a weak magnetic field. For comparison, Figure 4 shows samples of the $\rho(B)$ dependences in the range of $|B| \leq 0.1$ T for the semimetal ($V_g < V_{CNP}$) (*a*) and for the

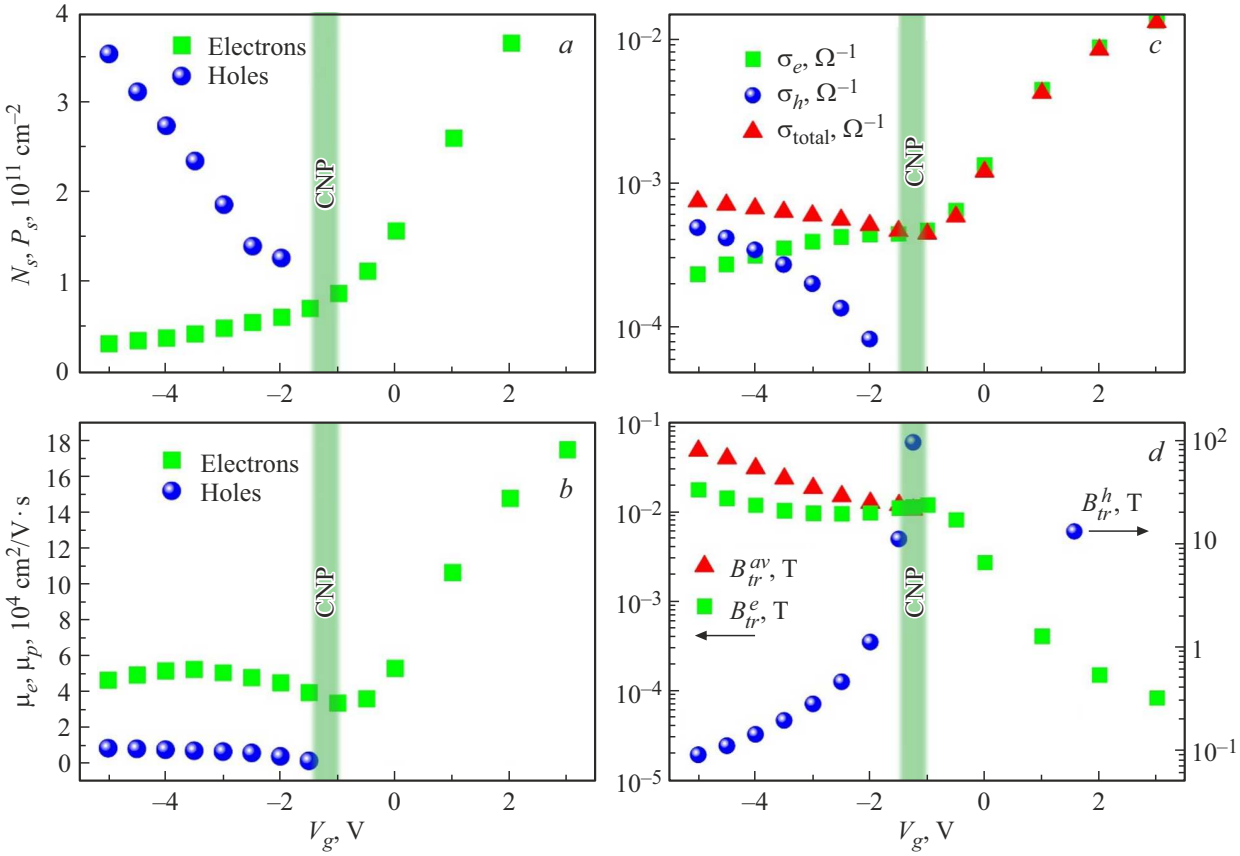

Figure 3. *a* — concentration of electrons and holes as a function of the gate voltage; *b* — mobility of electrons and holes as a function of the gate voltage gate voltage; *c* — partial (electron σ_e and hole σ_h) and total (σ_{total}) conductivities as functions of the gate voltage; *d* — dependences of the characteristic magnetic field B_{tr} separately for electrons B_{tr}^e, for holes B_{tr}^h and averaged magnetic field B_{tr}^{av} for bipolar transport in a 2D semimetal.

two-dimensional electron gas ($V_g > V_{CNP}$) (c) with similar resistivity values in zero magnetic field. An important distinguishing feature of the $\rho(B)$ behavior in the region of gate voltages of $V_g < V_{CNP}$ is the presence of a significant contribution from the classical Drude magnetoresistance, which is always present in a system with two types of charge carriers and which must be excluded if the study is focused on the interference corrections to conductivity. The latter was achieved by subtracting from the experimental dependence $\rho(B)$ (red curve in Figure 4, a) the classical magnetoresistance (blue curve in Figure 4, a), modeled using the Drude formula for the concentration and mobility of electrons and holes corresponding to a given gate voltage. The resulting dependence is shown in Figure 4, b. Such actions were required neither for $V_g \approx V_{CNP}$, where the contribution of classical magnetoresistance (MR) is weak, nor for $V_g > V_{CNP}$, where classical MR is absent. It can be seen from Figure 4 that in the studied samples, both in the state of two-dimensional electron gas and in the state of two-dimensional semimetal, a positive MR $\rho(B) - \rho(B = 0) > 0$ is observed, due to the suppression of interference corrections by the magnetic field (also known as anomalous MR (AMR) or weak antilocalization), which, as already noted, is typical for HgTe QWs of any thickness and is due to the rapid spin relaxation because to strong spin-orbit interaction in this system. Moreover, in contrast to a semimetal, where the quantum MR is always positive, for a two-dimensional electron metal, at a certain value of the magnetic field, a change in the MR sign from positive to negative could be observed. Also, it should be noted that for the same values of $\rho(B = 0)$ the AMR peak for the two-dimensional electron metal has a significantly smaller width than that for the semimetal. For the most distant values of the gate voltage, $V_g = +1$ V and $V_g = -5$ V, the difference in AMR peak width exceeds 2 orders of magnitude.

The experimental dependences $\rho(B)$ (taking into account the additional processing described above in the case of the semimetallic state, as well as after determining the zero of the magnetic field and symmetrization) were reduced to the following form: $\delta\sigma(B) = 1/\rho(B) - 1/\rho(0)$, which corresponds to the magnetoconductivity caused by the suppression of the interference correction to conductivity by the magnetic field. In Figures 5, a and 6, a series of similar dependences are shown for the semimetal ($V_g < V_{CNP}$) and for the electron metal, including the CNP region ($V_g \geq V_{CNP}$), respectively.

The choice of theory suitable for quantitative analysis of the dependences shown in Figures 5, a and 6, a is based on the magnitude of the characteristic magnetic field $B_{tr} = \hbar/2el$, where e is electron charge, and

$$l = \frac{\hbar}{e}\sqrt{\left(\frac{2\pi N_s}{g_v}\right)}\mu$$

is free path length, g_v is valley degeneracy. The determination of B_{tr}, which is trivial in the case of a two-dimensional electron metal, is not entirely obvious in the case of a two-dimensional semimetal, when two types of charge carriers — electrons and holes — are involved in the transport. In addressing this issue, we follow the approach proposed in [15], according to which the effective free path l_{av} in the case of a semimetal is determined by the sum of the natural free paths for electrons and holes, taken with weighting factors equal to the ratio of the partial contribution

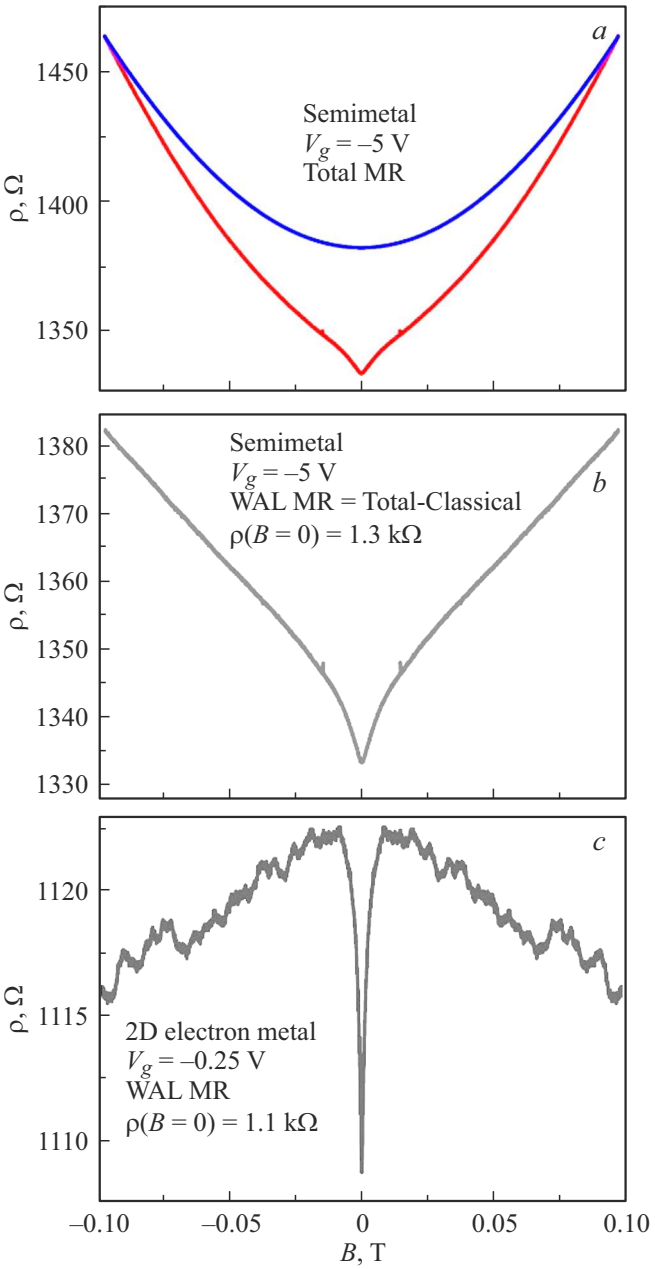

Figure 4. Samples of magnetofield dependences of resistance $\rho(B)$ for: a — semimetal, $V_g = -5$ V, $\rho(B = 0) = 1.3$ kOhm (red curve). Blue color shows the contribution of the classical MR for a given V_g; b — AMR for $V_g = -5$ V after subtracting the classical MR; c — AMR for 2D electron metal with $V_g = -0.25$ V, $\rho(B = 0) = 1.1$ kOhm. $T \approx 0.2$ K. (The colored version of the figure is available on-line).

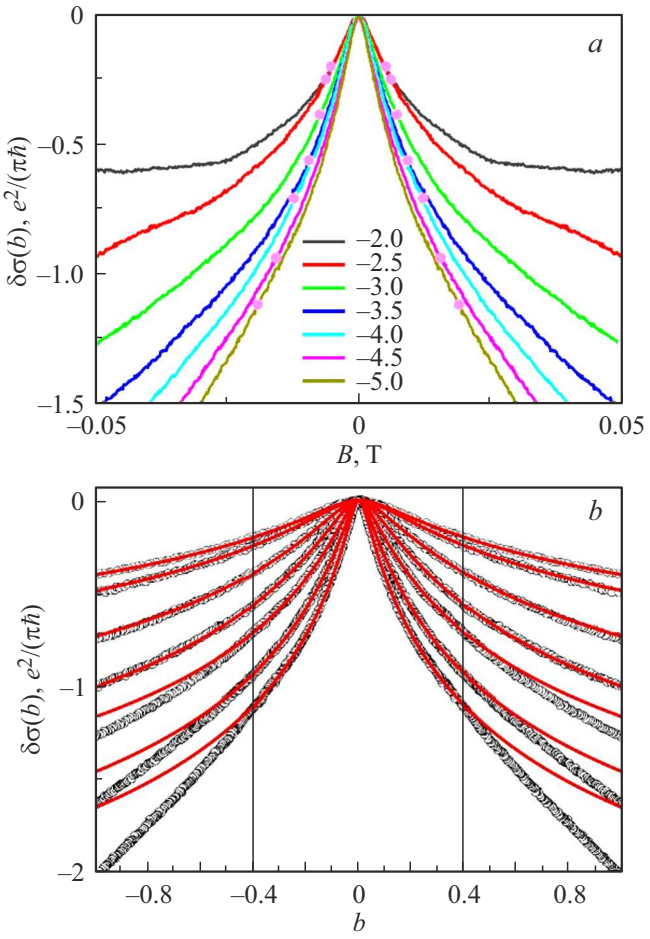

Figure 5. Dependences of $\delta\sigma(B) = \sigma(B) - \sigma(0)$ in the gate voltage range of $V_g = -5 - -2$ V (semimetal region): a — on the magnetic field B. Symbols indicate the values of B_{tr}^{av} corresponding to each curve; b — on $b = B/B_{tr}^{av}$ parameter. Symbols — experimental curves, solid lines — fitting by formula (1). Vertical lines indicate the range of the b parameter where the fitting was performed.

to the conductivity of a given type of carrier to the total conductivity:

$$l_{av} = l_e \frac{\sigma_e}{\sigma_{\text{total}}} + l_h \frac{\sigma_h}{\sigma_{\text{total}}}$$

(also, see Figure 3, c).

The values of B_{tr}^{av} obtained in this way for the semimetal, as well as the eigenvalues B_{tr}^{e} and B_{tr}^{h} for electrons and holes are shown as functions of the gate voltage in Figure 3, d. The values of $\pm B_{tr}^{av}$ for the semimetal in Figure 5, a and values of $\pm B_{tr}^{e}$ for electrons in Figure 6, a that correspond to the $\delta\sigma(B)$ dependences are indicated by round symbols superimposed on these dependencies. The results of recalculating the dependences of magnetoconductivity $\delta\sigma(B)$ into $\delta\sigma(b)$, where $b = B/B_{tr}^{av}$ for semimetal and $b = B/B_{tr}^{e}$ for electrons, are shown in by symbols in Figure 5, b and 6, b, respectively.

The use of a diffusion description of the magnetofield dependences of the interference correction to conductivity is considered acceptable if the part of the $\delta\sigma(B)$ dependence that is significant for analysis is within the limits of $|B| < B_{tr}$. In the case of a semimetal, the $\delta\sigma(B)$ dependences are antilocalization $\left(\frac{d\sigma(B)}{dB} < 0\right)$ in the entire range of magnetic fields, and the part of them that is within $|B| < B_{tr}^{av}$ (Figure 5) is quite sufficient to obtain reliable information about the system. In the case of a two-dimensional electron metal in magnetic fields of $|B_c| \geq 0.01$ T, a change in the sign of $\frac{d\sigma(B)}{dB}$ is observed with $|B_c| > B_{tr}^{e}$ for all dependences. However, due to the fact that the nature of this sign change is not completely clear, the consideration for electrons, as in the case of a semimetal, will be limited to the analysis of only the antilocalization part of the dependence, which is within the limits of $|B| < B_{tr}^{e}$. To increase the accuracy in all cases, comparison of theory with experiment was carried out in the range of $|b| \leq 0.4$, marked by vertical lines in Figure 5, b and 6, b. The test has shown that $\sim 25\%$ variations of the

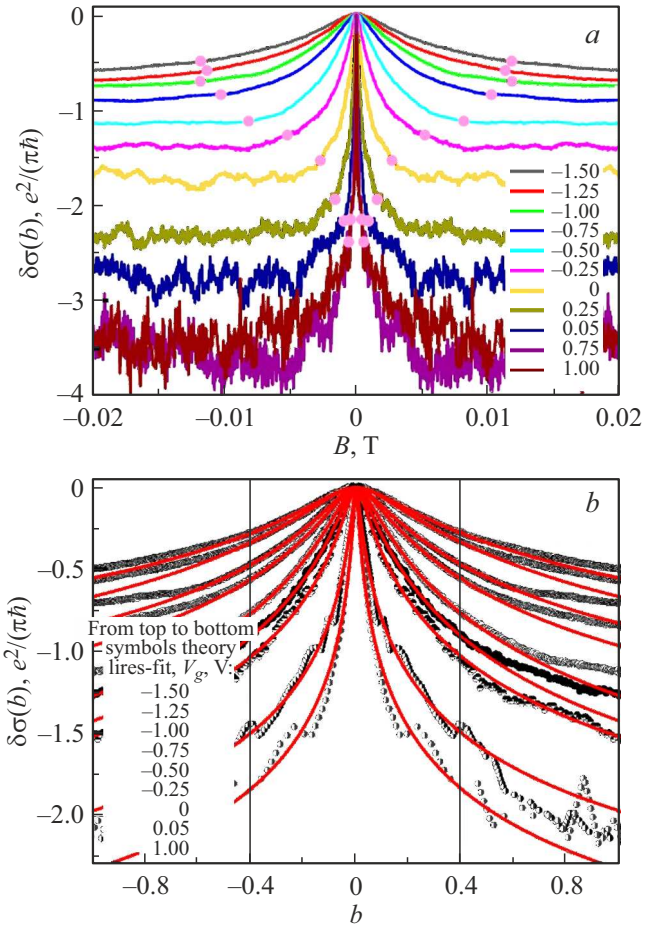

Figure 6. $\delta\sigma(B) = \sigma(B) - \sigma(0)$ dependences in the gate voltage range of $V_g = -1.5 - +1$ V (region of the charge neutrality point (CNP) and 2D electron metal): a — on the magnetic fields B. Symbols indicate the values corresponding to each curve B_{tr}^{e}; b — on the $b = B/B_{tr}^{e}$ parameter. Symbols — experimental curves, solid lines — fitting by formula (1). Vertical lines indicate the range of the b parameter where the fitting was performed.

$|b|$ range used for the comparison with the theory have no effect on the values of the extracted parameters.

To describe the antilocalization dependence $\delta\sigma(b)$ in the diffusion limit $\left(\frac{d\sigma(b)}{db} < 0 \text{ at } |b| < 1\right)$, the standard expression [16,17] is used:

$$\Delta\sigma(b) = \alpha G_0 \mathscr{H}\left(\frac{\tau}{\tau_\phi}, b\right)$$

$$\mathscr{H}(x, y) = \psi\left(\frac{1}{2} + \frac{x}{y}\right) - \psi\left(\frac{1}{2} + \frac{1}{y}\right) - \ln(x), \quad (1)$$

where

$$G_0 = \frac{e^2}{2\pi^2\hbar},$$

$\psi(x)$ is digamma function, and the prefactor α and the ratio of the pulse relaxation transport time to the phase coherence time $\beta = \tau_\phi/\tau$ are used as fitting parameters.

Figure 5, *b* and 6, *b* show the experimental curves (symbols) and the results of fitting to them (solid lines) using formula (1). It can be seen that the diffusion theory of interference corrections to conductivity describes well all experimental dependences in the selected range of $|b| \leq 0.4$.

Figure 7, *a* and *b* show dependences of the α and $\beta = \tau_\phi/\tau$ parameters on the gate voltage obtained as a result of fitting. Let's first consider the behavior of the α parameter. It is well known that the value of the prefactor α in the case of weak localization should be equal to 1, and in the case of weak antilocalization it should be $-1/2$. It can be seen in Figure 7, *a* that in the semimetal region α increases monotonically from ≈ -0.7 to ≈ -0.3 immediately before the charge neutrality point. In the vicinity of CNP and immediately beyond this point α decreases to almost the same values as those observed in the semimetal region at minimum electron concentrations. Finally, under conditions of pure electron conductivity, α reaches the value of $-1/2$ expected in the case of weak antilocalization. Typically, in a situation where several different groups of charge carriers are present in the system, as, for example, in [8,9,11,12], the following reasoning is used to describe the behavior of α. If the frequency of carrier transitions between groups is low compared to $1/\tau_\phi$, then these groups can be considered as independent subsystems, whose contributions to the experimentally determined α are summed up: $\alpha = -0.5 - 0.5 = -1$. If, on the contrary, the transition frequency is high ($\gg 1/\tau_\phi$), then the difference between the groups is leveled out and $\alpha = -0.5$, as in a system with one group of carriers. The above is obviously true for groups of carriers with the same sign. It is not entirely clear whether similar reasoning is applicable to semimetal, where electrons and holes are simultaneously present. The behavior in Figure 7, *a* in the semimetal region can be interpreted as follows: the largest absolute value of α coincides with regions where the concentrations of electrons and holes are very different. This may indicate that under these conditions the frequency of transitions between these groups of carriers is minimal,

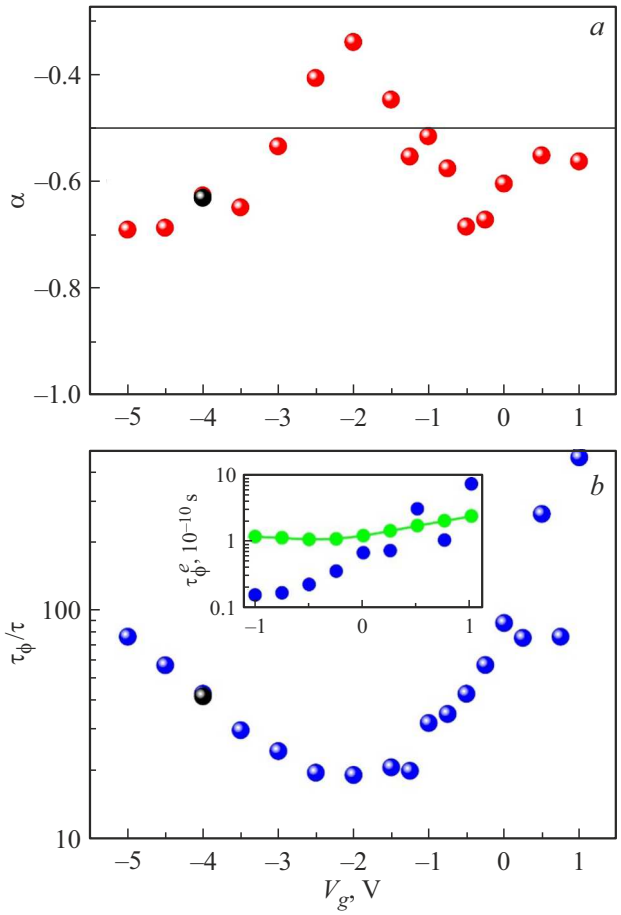

Figure 7. $\alpha(a)$ and τ_ϕ/τ parameters (b) extracted from the fitting (see Figure 5, 6) depending on the gate voltage. The inset to (b) shows $\tau_\phi^e(V_g)$ dependences for electrons: the experimental dependence (blue symbols) and the theoretical dependence (green symbols), plotted using formula (2).

while it increases as the concentrations of electrons and holes in the vicinity of CNP equalize.

As for the interpretation of the $\beta = \tau_\phi/\tau$ parameter behavior (Figure 7, *b*), in the semimetal region it is complicated by the fact that in this case both τ and τ_ϕ are complex combinations of corresponding quantities for electrons and holes. In the region of two-dimensional electron metal, on the contrary, the obtained values of β make it possible to immediately determine the dependence of τ_ϕ^e on the gate voltage for electrons (see inset to Figure 7, *b*). The same figure shows the theoretical dependence $\tau_\phi(V_g)$ obtained using the following formula [18]

$$\frac{1}{\tau_\phi} \approx \frac{k_B T}{\hbar} \frac{e^2/\hbar}{\sigma} \ln\left(\frac{\sigma}{e^2/\hbar}\right). \quad (2)$$

It can be seen that far from the CNP in the region of high electron concentrations, the experimental τ_ϕ^e values are well consistent with the theory. However, as the electron concentration decreases with approaching the CNP, the experimental dependence $\tau_\phi^e(V_g)$ drops significantly below

the theoretical one, and the difference reaches almost an order of magnitude at $V_g \approx V_{\mathrm{CNP}}$. This behavior may indicate that even a slight presence of holes, not directly detected in the transport, can significantly limit the phase coherence time of electrons.

4. Conclusion

Thus, in this study, interference corrections to conductivity in a two-dimensional semimetal based on 20 nm HgTe QW — a binary two-dimensional system, including subsystems of degenerate electrons and holes simultaneously participating in transport — were investigated for the first time. To enhance the relative magnitude of the quantum correction to the measured resistance, QWs were used, in which additional disorder was created using bulk doping that reduces conductivity of the system. Magnetotransport measurements carried out in a wide range of electron and hole concentrations in a two-dimensional semimetal, as well as in the region of a two-dimensional electron metal, revealed the presence of a positive MR, indicating a high intensity of spin relaxation in the system under study. A quantitative analysis of the data obtained indicates a possible correlation between the intensity of carrier transitions between the subsystems of electrons and holes in a two-dimensional semimetal with the ratio of carrier concentrations in these subsystems.

Funding

The study was supported by the Ministry of Science and Higher Education of the Russian Federation.

Conflict of interest

The authors declare that they have no conflict of interest.

References

[1] L.G. Gerchikov, A. Subashiev. Phys. Status Solidi B, **160**, 443 (1990).
[2] M. Konig, S. Wiedmann, C. Brune, A. Roth, H. Buhmann, L.W. Molenkamp, X.-L. Qi, S.-C. Zhang. Science, **318**, 766 (2007).
[3] O.A. Pankratov, UFN **188**, 1226, (2018). (in Russian).
[4] M.V. Durnev, S.A. Tarasenko. Ann. Phys. (Berlin), **531**, 1800418 (2019).
[5] H. Plank, S.D. Ganichev. Solid-State Electron., **147**, 44 (2018).
[6] E.B. Olshanetsky, Z.D. Kvon, G.M. Gusev, A.D. Levin, O.E. Raichev, N.N. Mikhailov, S.A. Dvoretsky. Phys. Rev. Lett., **114**, 126802 (2015).
[7] E.B. Olshanetsky, Z.D. Kvon, G.M. Gusev, N.N. Mikhailov, S.A. Dvoretsky, J.C. Portal. JETP Lett., **91**, 347 (2010).
[8] G.M. Minkov, A.V. Germanenko, O.E. Rut, A.A. Sherstobitov, S.A. Dvoretski, N.N. Mikhailov. Phys. Rev. B, **85**, 235312 (2012).
[9] G.M. Minkov, A.V. Germanenko, O.E. Rut, A.A. Sherstobitov, S.A. Dvoretski, N.N. Mikhailov. Phys. Rev. B, **91**, 205302 (2015).
[10] D.A. Kozlov, Z.D. Kvon, N.N. Mikhailov, S.A. Dvoretsky. JETP Lett., **96**, 730 (2013).
[11] M.L. Savchenko, D.A. Kozlov, Z.D. Kvon, N.N. Mikhailov, S.A. Dvoretsky. JETP Lett., **104**, 302 (2016).
[12] M.L. Savchenko, D.A. Kozlov, N.N. Mikhailov, S.A. Dvoretsky, Z.D. Kvon. Physica E, **129**, 114624 (2021).
[13] Z.D. Kvon, E. Olshanetsky, D.A. Kozlov, N.N. Mikhailov, S.A. Dvoretskii. JETP Lett., **87**, 502 (2008).
[14] Z.D. Kvon, E.B. Olshanetsky, D.A. Kozlov, E.G. Novik, N.N. Mikhailov, S.A. Dvoretsky, Fizika nizkikh temperatur, **37**, 258 (2011). (in Russian).
[15] D.D. Bykanov, A.M. Kreshchuk, S.V. Novikov, T.A. Polyanskaya, I.G. Savel'ev. Semiconductors, **32**, 985 (1998).
[16] S. Hikami, A.I. Larkin, Y. Nagaoka. Prog. Theor. Phys., **63**, 707 (1980).
[17] H.-P. Wittmann, A. Schmid. J. Low Temp. Phys., **69**, 131 (1987).
[18] B.L. Altshuler, A.G. Aronov, D.E. Khmelnitsky. J. Phys. C, **15**, 7367 (1982).

Translated by Y.Alekseev